Appl. Phys. B 63, 585–591 (1996)

Applied Physics B Lasers and Optics

A high average power rotating hollow cylinder Nd:glass laser

F. Zhou*, G. Huang, S. Gu

Shanghai Institute of Optics and Fine Mechanics, Academia Sinica, P.O. Box 800-216, Shanghai 201800, China
(Fax + 86-21/952-8885)

Received: 22 June 1995/Accepted: 11 June 1996

Abstract. The rotating hollow cylinder glass laser is one of the approaches for the generation of high average output powers scaling to kilowatt levels from solid-state laser materials. An analytical solution of the heat conduction equation is presented for a thin wall, infinitely long glass medium, with boundary conditions given by Newton's law of cooling. The theoretical result is applied to predict thermal effects of this geometry which ultimately limit the laser performance, and the design of such a laser. A flashlamp pumped rotating Nd-doped phosphate glass hollow cylinder laser has been demonstrated. An average power output of 300 W has been achieved at 3.8% slope efficiency and 2.6% overall efficiency. Our investigation shows that the development of a kilowatt average power rotating cylinder laser is feasible.

PACS: 42.55; 42.60

Nd:glass is a laser material that has been developed extensively for high peak power laser systems [1]. Unlike most laser crystals, high optical quality Nd:glass is relatively inexpensive and can be fabricated in different sizes and shapes. This material is also less sensitive to the self-quenching effect as the concentration of the active ions increases. Flashlamp pumping combined with the large saturation fluence of Nd:glass enables the production of high energy as well as high peak power laser pulses. However, the poor thermal conductivity and the low mechanical strength of glass, which results in thermally induced optical distortions and fractures, have previously limited the usefulness of Nd:glass in high average power laser applications. While the thermal lensing and stress-induced birefringence can be controlled and compensated for to some extent [2–6], the thermal stress fracture of glass is a fundamental limiting factor.

The moving-slab-geometry laser was first proposed by Kane and Byer [7–9] for the high average power operation of Nd:glass. By moving a piece of glass medium, the thermal load and cooling take place over a much larger area while the gain is concentrated in the small pumped volume. This results in a gain enhancement and greater ease of extracting the laser energy, while maintaining average power scaling as the area of the slab. Possible moving-slab structures include a linearly moving rectangular slab, a rotating disk and a rotating cylinder.

Recently a moving rectangular slab Nd:glass laser with an average output power of 43.8 W at 2.06% slope efficiency has been demonstrated [10]. One disadvantage of this system is the nonuniform heating of the slab due to the discontinuity of motion of the rectangular slab at turning points near both sides and the unavoidable heat transfer along these sides. The continuous-wave operation of a diode-pumped rotating Nd:glass disk laser has also been reported to give an average power output of 0.55 W with 2 W of absorbed pumped power [15]. Because of the limited gain length, a laser operating at high average power levels will probably require a number of rotating disks, which leads to the complexity of the mechanical design and high costs.

A hollow cylinder of Nd:glass rotating around its axis combines the advantage of continuous rotation and uniform heating. Although non-rotating Nd:glass [11, 12] and Nd:YAG [13, 14] hollow cylinder lasers have been reported, there are few papers on thermal effects and the laser performance of a rotating hollow cylinder laser. In this paper we present an analytical model for pump-induced thermal effects of a rotating hollow cylinder laser. The theoretical results are compared to experimental measurements, which shows a good agreement. We also report the design and demonstration of a rotating Nd:glass hollow cylinder laser providing an average power output of 300 W at 2.6% overall efficiency. Our investigations allow important conclusions to be drawn, concerning host glass selection, pump power limitation and laser design considerations.

**Present address*: School of Science, Nanyang Technological University, 469 Bukit Timah Road, Singapore 259756
(Fax: + 65-469/8952, E-mail: nfzhou@ntuvax.ntu.ac.sg)

1 Theory

1.1 Temperature distribution

As shown in Fig. 1, a hollow circular Nd:glass cylinder of length L and inside and outside radii, a and b, rotates around its axis z with a constant angular velocity ω. The cylinder is pumped and cooled through both the inner and outer surfaces with a thermal power loading per unit volume Q and a surface heat transfer coefficient H. The ends are uncooled and the end effects are neglected, so the cylinder is considered to be infinitely long. The initial temperature of the cylinder and coolant is assumed to be 0 °C. The temperature distribution $\tau(r,\theta,t)$ within the hollow cylinder is governed by the following heat conduction equation described in a cylindrical coordinate system [16]

$$\frac{\partial^2\tau}{\partial r^2}+\frac{1}{r}\frac{\partial\tau}{\partial r}+\frac{1}{r^2}\frac{\partial^2\tau}{\partial\theta^2}+\frac{Q}{k}-\frac{\rho c}{k}\left(\frac{\partial\tau}{\partial t}-\omega\frac{\partial\tau}{\partial\theta}\right)=0, \tag{1}$$

with boundary conditions given by Newton's law of cooling

$$\left.\frac{\partial\tau}{\partial r}\right|_{r=a,b}=\pm h_{a,b}\tau\Big|_{r=a,b} \tag{2}$$

and an initial condition

$$\tau(r,\theta,0)=0, \tag{3}$$

where $h_i=H_i/\kappa(i=a,b)$, and c, ρ, κ are the specific heat, density and thermal conductivity of a laser glass medium, respectively.

In the general case, (1)–(3) can be solved numerically. However, with the following assumptions, an analytical solution is possible. We assume that

(1) since the cylinder rotates at constant angular velocity, thermal loading is uniformly dissipated and the heat flow is strictly radial, i.e.,

$$\frac{\partial Q}{\partial\theta}=0 \quad\text{and}\quad \frac{\partial\tau}{\partial\theta}=0;$$

(2) because the thickness $(b-a)$ of the cylinder is much smaller than the inside radius a, the internal heat is uniformly generated along radial direction,

$$\frac{\partial Q}{\partial r}=0;$$

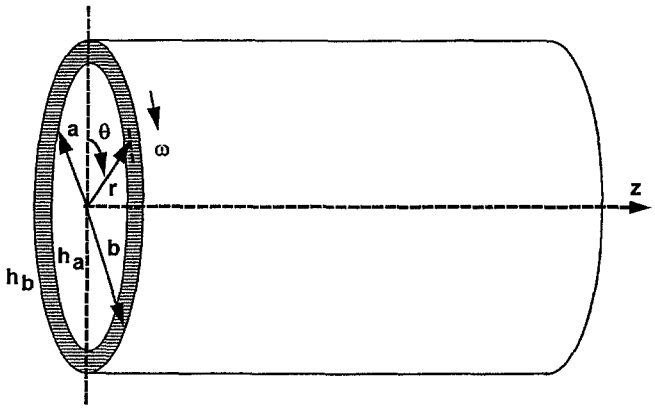

Fig. 1. Geometry of a rotating hollow cylinder

(3) the pump pulse waveform is rectangular with a width of t_1 and a cycle of t_0, and the power density dissipated as heat in the thin wall, hollow cylinder can be expressed as:

$$Q(t)=\begin{cases}Q_0, & Nt_0\le t<(Nt_0+t_1),\\ 0, & (Nt_0+t_1)\le t<(N+1)t_0,\end{cases}$$

where $N=0,1,2,\ldots$, is the pumping pulse order.

Under the above assumptions, analytical solutions of the heat conduction equation, with a cw pump and a repetitively pulsed pump, have been obtained by applying the method of separation of variables and Duhamel's theorem [17]. The thermal time constant of the cylinder is defined as:

$$t_c=\frac{\rho c}{\kappa\mu_1^2},$$

where μ_1 is the first positive root of the following equations $(n=1,2,3,\ldots)$;

$$\frac{h}{\sqrt{h^2+\mu_n^2}}=\sin\left[\frac{\mu_n}{2}(b-a)\right].$$

For an N_{2135} phosphate glass cylinder of $a=10.8$ cm, $b=1.6$ cm, $\kappa=0.0053$ W/(cm °C), $c=0.75$ J/(g °C), $\rho=3.4$ g/cm^3, and $h=100$ cm^{-1} for the contacted water cooling [18], the thermal time constant t_c is 32 s. When $t\ge t_c$ the influence of the first N pump pulses has disappeared and a steady-state thermal equilibrium is established. Thus for large values of the time and $Nt_0\gg t_c$, the general expression of the radial temperature distribution $\tau(r,t)$ is

$$\tau(r,t)=\begin{cases}\tau(r)+\dfrac{Q_0}{4\kappa}\displaystyle\sum_{n=1}^{\infty}B_nR(\mu_nr)\frac{e^{t_0/t_n}-e^{t_1/t_n}}{1-e^{t_0/t_n}}e^{-t/t_n}, & Nt_0\le t<Nt_0+t_1,\\ \tau(r)+\dfrac{Q_0}{4\kappa}\displaystyle\sum_{n=1}^{\infty}B_nR(\mu_nr)\left(\frac{e^{t_0/t_n}-e^{(t_0-t_1)/t_n}}{1-e^{t_0/t_n}}e^{-t/t_n}-1\right), & Nt_0+t_1\le t\le(N+1)t_0,\end{cases} \tag{4}$$

and the heat transfer coefficient on the inner surface is the same as that on the outer surface,

$$H_a=H_b=H;$$

where

$$\tau(r)=\tau_0-\frac{Q_0}{4\kappa}\left(r^2-C^2\ln\frac{r}{a}\right) \tag{5}$$

is the steady-state temperature distribution of a cw hollow cylinder laser with

$$\tau_0 = \frac{Q_0}{4\kappa}\left(a^2 - \frac{2a}{h} + \frac{C^2}{ah}\right) \quad \text{and}$$

$$C^2 = \frac{2a + 2b + h(b^2 - a^2)}{\frac{1}{a} + \frac{1}{b} + h\ln\left(\frac{b}{a}\right)}.$$

B_n, β_n, and t_n are constants:

$$B_n = \frac{\pi\mu_n}{(h^2 + \mu_n^2)(\beta_n^2 - 1)}\left[\frac{4h}{\mu_n^2}(\beta_n - 1) + C^2\left(h\ln\frac{b}{a} + \frac{\beta_n}{b} + \frac{2 - \beta_n}{b}\right) - (b + a)(hb - ha + 2)\right];$$

$$\beta_n = \frac{hJ_0(\mu_n a) + \mu_n J_1(\mu_n a)}{hJ_0(\mu_n b) - \mu_n J_1(\mu_n b)}, \quad t_n = \frac{\rho c}{\kappa\mu_n^2},$$

and

$$R(\mu_n r) = [\mu_n J_1(\mu_n a) + hJ_0(\mu_n a)]\, Y_0(\mu_n r) - [\mu_n Y_1(\mu_n a) + hY_0(\mu_n a)]\, J_0(\mu_n r)$$

is the combinations of the zero and the first order Bessel's functions of the first ((J_0, J_1) and second kind (Y_0, Y_1). As can be seen from (4), the steady-state temperature distribution of a thin wall hollow cylinder in the repetitively pulsed mode of operation is equal to the steady-state temperature distribution at cw operation $\tau(r)$ plus a periodic disturbance which depends on the pump pulse width t_1, cycle t_0 and thermal properties t_n. For an N_{2135} phosphate glass cylinder of $a = 10.8$ cm, $b = 11.6$ cm, $\kappa = 0.0053$ W/(cm °C), $c = 0.75$ J/(g °C), $\rho = 3.4$ g/cm^3 and $h = 100$ cm^{-1}, the peak to peak variation in temperature is calculated to be about 1% in the case of $t_1 = 0.5$ ms and $t_0 = 1$ s. When the pump repetition rate is increased from 1 to 5 Hz, variance decreases to less than 0.3%. Therefore, the temperature variation is negligible when the pump repetition rates are equal to or higher than 1 Hz, and the overall steady-state temperature response as a function of time can be considered to be the same as that in the cw mode of operation.

As can be seen from (5), the average temperature $\bar{\tau}$ is

$$\bar{\tau} = \frac{2}{b^2 - a^2}\int_a^b \tau(r)\, r\, \mathrm{d}r = \frac{Q_0}{8\kappa}\left(\frac{2b^2C^2}{b^2 - a^2}\ln\frac{b}{a} + a^2 - b^2 - C^2\right) + \tau(a),$$

where $\tau(a)$ is the temperature on the inner surface of the cylinder;

$$\tau(a) = \frac{Q_0}{4\kappa h}\left(\frac{C^2}{a} - 2a\right).$$

The highest temperature occurs near the centre of the thickness, at $r = C/\sqrt{2}$,

$$\tau_{\max} = \tau(r = C/\sqrt{2}) = \frac{Q_0}{4\kappa}\left(a^2 - \frac{C^2}{2} + C^2\ln\frac{\sqrt{2C}}{2a}\right) + \tau(a).$$

When the surface heat transfer coefficient h increases, these temperatures decrease quickly for a cylinder of the same parameters.

1.2 Thermal stresses and pump power limit

The temperature gradient of the cylinder is responsible for high stresses presented in the material. The radial σ_{rr}, tangential $\sigma_{\theta\theta}$, and axial σ_{zz} stress component in an isotropic hollow cylinder caused by a temperature distribution $\tau(r)$ are determined by [19]

$$\sigma_{rr}(r) = \frac{\kappa}{2M_S}\left[\left(1 - \frac{a^2}{r^2}\right)\bar{\tau} - \overline{\tau(r)}\right],$$

$$\sigma_{\theta\theta}(r) = \frac{\kappa}{2M_S}\left[\left(1 - \frac{a^2}{r^2}\right)\bar{\tau} + \overline{\tau(r)} - 2\tau(r)\right], \tag{6}$$

$$\sigma_{zz}(r) = \frac{\kappa}{M_S}\left[\overline{\tau(r)} - \tau(r)\right],$$

where

$$\overline{\tau(r)} = \frac{2}{r^2}\int_a^r \tau(r)\, r\, \mathrm{d}r$$

and $M_S = (1 - \nu)\kappa/\alpha E$ is the material figure of merit with ν the Poisson's ratio, α the thermal coefficient of expansion, and E Young's modules. Substituting (5) into (6), we have

$$\sigma_{rr}(r) = \frac{Q_0}{16M_S}\left(r^2 - \Lambda\frac{a^2b^2}{r^2} - 2C^2\ln\frac{r}{a} + \Gamma^2\right),$$

$$\sigma_{\theta\theta}(r) = \frac{Q_0}{16M_S}\left(3r^2 + \Lambda\frac{a^2b^2}{r^2} - 2C^2\ln\frac{r}{a} + \Gamma^2 - 2C^2\right), \tag{7}$$

$$\sigma_{zz}(r) = \frac{Q_0}{16M_S}\left(2r^2 - 2C^2\ln\frac{r}{a} + \Gamma^2 - C^2\right),$$

where

$$\Lambda = \frac{2C^2}{b^2 - a^2}\ln\frac{b}{a} - 1 \quad \text{and} \quad \Gamma^2 = \Lambda b^2 - a^2.$$

As the inner radius $a \to 0$, we have $C = 0$, $\Lambda = 1$, $\Gamma^2 = b^2$, $C^2\ln(r/a) = b^2$. Equation (7) gives stresses in a rod, as previously shown [20]:

$$\sigma_{rr}(r) = \frac{Q_0}{16M_S}(r^2 - b^2),$$

$$\sigma_{\theta\theta}(r) = \frac{Q_0}{16M_S}(3r^2 - b^2), \tag{8}$$

$$\sigma_{zz}(r) = \frac{Q_0}{8M_S}(2r^2 - b^2).$$

The maximum stress occurs on the outer surface of the cylinder

$$\sigma_S = \frac{Q_0}{8M_S}\xi^2.$$

where

$$\xi^2 = \frac{(\Lambda+3)b^2 + (\Lambda-1)a^2}{2} - \left(1 + \ln\frac{b}{a}\right) C^2.$$

As the power dissipated in the cylinder is increased, the tension on the cylinder outside surface reaches the material stress limit σ_{max}, resulting in the formation of stress fracture. The maximum thermal power density dissipated in the cylinder is ($\sigma_S = \sigma_{max}$)

$$Q_{max} = \frac{8R_S}{\xi^2}, \tag{9}$$

where $R_S = M_S\sigma_{max}$ is the thermal shock parameter of a material. As $a \to 0$, thus $\xi^2 = b^2$, we get the thermal power density limit for a rod of radius b:

$$Q^r_{max} = \frac{8R_S}{b^2}. \tag{10}$$

As $a \to \infty$, we have

$$\lim_{a\to\infty} \xi^2 = \frac{2}{3}(b-a)^2,$$

which gives the thermal power density limit for a slab of thickness $t = (b - a)$,

$$Q^s_{max} = \frac{12R_S}{t^2}. \tag{11}$$

Combining (9)–(11), the maximum thermal power density for different gain medium geometries can be expressed as

$$Q_{max} = \frac{R_S}{K_S^2}, \tag{12}$$

where K_S is a parameter depending on the laser medium structure. For a rod, $K_S^2 = b^2/8$; for a hollow cylinder, $K_S^2 = \xi^2/8$; and for a slab, $K_S^2 = t^2/12$.

Figure 2 shows average temperature $\bar{\tau}$, maximum temperature τ_{max}, and inner surface temperature $\tau(a)$ of an N_{2135} phosphate glass cylinder at cw operation versus surface heat transfer h and at $Q_0 = 1$ W/cm^3. The inner and outer radii a, b are 5.8 and 6.6 cm, respectively. Figure 2 also shows the calculated maximum thermal power density Q_{max} of the same cylinder as a function of the surface heat transfer h. When h increases, Q_{max} goes up slowly while the temperatures decreases very quickly.

The maximum pump power density P_{max} is

$$P_{max} = R_S/K_S^2\eta_H, \tag{13}$$

where η_H is the heating efficiency relating the electrical input power to the power dissipated as heat in the cylinder. Table 1 summarises physical properties of different types of Nd:glass, and calculations of maximum thermal power density P_{max} for different laser medium geometries which have the same thermal conductive path. In these calculations, $\eta_H = 11\%$ is used [22]. As expected, the thermal power density for a large diameter thin wall hollow cylinder is very close to that for a slab of the same thickness.

We define a safe factor to be such that the designed maximum pump power is kept at 50% of the pump power when the fractures actually happen. In order to determine

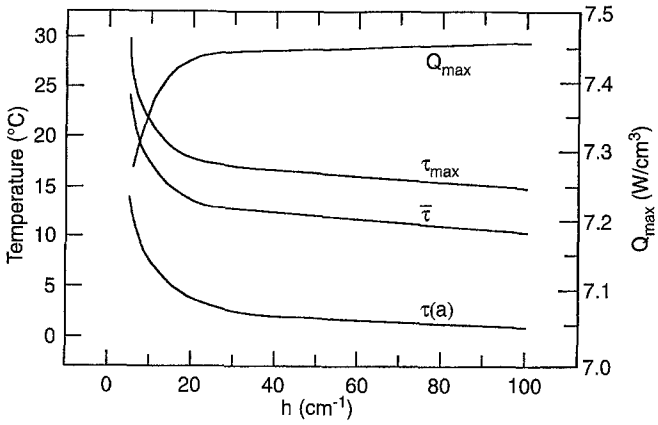

Fig. 2. Maximum temperature τ_{max}, average temperature $\bar{\tau}$, and inner surface temperature τ(a) at $Q_0 = 1$ W/cm^3 vs different surface heat transfer conditions. The maximum thermal power density Q_{max} which the cylinder can tolerate is also shown as a function of h

Table 1. Physical properties of different types of Nd:glass and maximum thermal power densities for different geometries [21]:

	Silicate		Phosphate	
	N_{335}	N_{1035}	N_{2135}	LHG-5
ν	0.23	0.22	0.27	0.24
ρ(g/cm^3)	2.51	2.52	3.40	2.68
$p(\times 10^{-6}$/°C)	4.9	4.6	6.0	
$q(\times 10^{-6}$/°C)	0.9	1.1	0.5	
$\beta_e(\times 10^{-6}$/°C)	1.64	0.80	−5.30	
$\kappa(\times 10^{-3}$ W/(cm °C))	10.1	14.1	5.3	7.7
$\alpha(\times 10^{-6}$/°C)	8.0	8.9	12.0	8.6
$E(\times 10^5$ kg/cm^2)	7.60	7.50	5.64	6.93
$M_S(\times 10^{-3}$ W cm/kg)	1.28	2.02	0.57	0.99
σ_{max}(kg/cm^2)	940	890	650	990
R_S(W/cm)	1.2	1.8	0.4	0.98
Q^r_{max}(W/cm^3) $b = 0.4$ cm	60.0	73.5	20.0	49.0
Q^s_{max}(W/cm^3) $t = 0.8$ cm	22.6	27.7	7.5	18.5
Q_{max}(W/cm^3) $a = 5.8$ cm, $t = 0.8$ cm	22.2	27.2	7.4	18.1

k_C, both silicate N_{335}, N_{1035} and phosphate N_{2135} Nd:glass have been used for stress fracture tests [6, 23]. Due to optical surface scratches, material defects, residual stresses and temperature nonuniformity, the measured maximum thermal power density is less than the calculated value. Our experiments show that the fractures occur at (80 ± 5)% of the calculated values given by (13), so we take the value of k_C as 0.4 and the following pump power density limit is used for the design of a cylinder laser

$$\bar{P}_{max} = k_C \times R_S/K_S^2\eta_H. \tag{14}$$

1.3 Thermal change of refractive index

The total variations of refractive index for radial r and tangential θ polarisation in a glass hollow cylinder due to

the temperature gradient and stresses are given by [24, 25]

$$\Delta n_{r,\theta} = n^0 + \frac{pQ_0}{4\kappa}\left(a^2 + C^2 \ln\frac{r}{a} - r^2\right) \pm \frac{qQ_0}{8\kappa}\left[C^2 - r^2 - (a^2 + \Gamma^2)\frac{a^2}{r^2}\right]$$

where

$$n^0 = \frac{Q_0}{8\kappa}(\beta_e + p)(2a^2 + \Gamma^2 - C^2);$$

β_e is the temperature coefficient of refraction index, ρ is the thermal optic coefficient, q is the stress birefringence coefficient of a medium. These values for different types of Nd:glass are also listed in Table 1.

For an unpolarised beam, the thermal change of refractive index Δn is approximately obtained from

$$\Delta n = \frac{(\Delta n_r + \Delta n_\theta)}{2} = n^0 + \frac{pQ_0}{4\kappa}\left(a^2 + C^2 \ln\frac{r}{a} - r^2\right). \quad (15)$$

The maximum difference of refractive index of the hollow cylinder occurs at $r = C/\sqrt{2}$,

$$\Delta n(r) = \frac{pQ_0}{4\kappa}\left(a^2 + C^2 \ln\frac{\sqrt{2}C}{2a} - \frac{C^2}{2}\right). \quad (16)$$

The similar expressions for a rod can be derived from (15) and (6) by assuming $a \to 0$,

$$\Delta n = \frac{Q_0(\beta_e + p)}{8\kappa} b^2 + \frac{pQ_0}{4\kappa}(b^2 - r^2),$$

$$\Delta n(r) = \frac{pQ_0}{4\kappa} b^2.$$

A Mach-Zehnder interferometer with a glass cylinder in one arm has been used to measure the optical distortion at different average pump power [25]. The experimental measurement of the steady-state refractive index profiles Δn along the cylinder thickness direction r at different pump densities is given in Fig. 3, which shows a good agreement with the results calculated according to (16). The experiment also reveals that the distribution of thermal loading Q_0 along radial direction is not uniform when the glass is highly doped with Nd^+ ions.

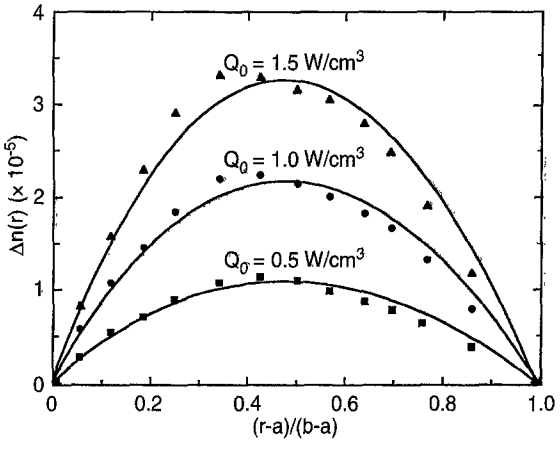

Fig. 3. Experimental (*scatters*) and theoretical (*solid lines*) results of the steady-state refractive index profiles Δn against the normalised cylinder thickness at different pump densities Q_0. The deviation from the theoretical prediction is mainly due to the non-uniform distribution of the thermal loading

2 Laser experiments

A schematic of the basic laser head design is shown in Fig. 4. The glass cylinder used is made of Nd doped N_{2135} phosphate glass with a doping percentage of 3.5% (wt). This doping percentage is chosen as a trade-off between good pump light absorption and uniform internal heating. The cylinder has a length of 32 cm, an inner diameter and a thickness of 11.6 and 0.8 cm, respectively. The length of the cylinder receiving pump radiation is 26 cm, and the two ends are shaded to minimise the end effects, which gives a total effective volume of 810 cm^3. The device is

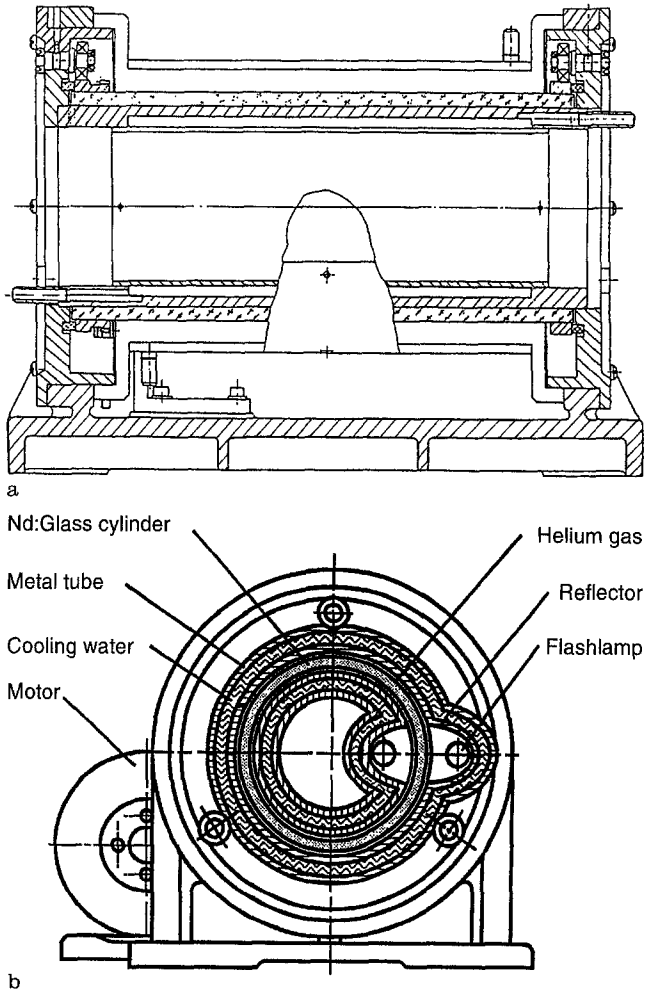

Fig. 4a, b. Schematic diagram of the rotating cylinder laser design (drawn not to scale: (**a**) the longitudinal cross section; (**b**) the transverse cross section)

designed to maintain the surface stress σ_S at a safe level far below the fracture stress σ_{max} to prevent physical damage. It is important to provide uniform pump illumination and cooling of the cylinder to minimise optical distortions of the laser [26].

The cylinder is pumped by two 23 cm arc-length 1.2 cm diameter xenon flashlamps through both the inner and outer surface. The flashlamp with a cerium-doped quartz envelope is cooled by a turbulent flow of water between the envelope and a water jacket at 30 l/min rate, which leads to an average water temperature increase of 3.5 °C at the average input power of 12 kW. Two silver coated single elliptical reflectors with 3.2 cm open apertures are used to focus the lamps to the cylinder. The cylinder rotates around its axis between two water-cooled metal tubes. The gap between the glass cylinder and metal tubes is held at 0.2 mm and filled with static helium gas at atmospheric pressure, which is not sealed. A consumption of helium gas of 5 l per hour is needed to operate the laser. The thin layer helium gas acts reasonably well as heat-conducting medium [27]. The calculated thermal time constant for this cylinder cooled by the thin layer of helium gas is about 48 s. The thin metal tube is cooled by a water flow at 5 l/min rate. The average temperature increase of the water coolant is 2.0 °C at 12 kW average input power.

The cylinder is driven by a computer controlled step motor and the rotating speed is adjustable. Each rotation of $\pi/10$ of the cylinder provides a trigger signal to a laser power supply to discharge the stored energy into the flaslamps, resulting in 20 laser pulses for one round trip. The pump pulse has a duration of 0.5 ms (FWHM), which is greater than the fluorescent decay time of 310 μs for N_{2135} glass. The laser resonator consists of a 80 cm long cavity formed with a 5 m radius concave high reflector back mirror, which is 30 cm away from one end of the glass cylinder, and a 70% reflectivity flat output coupler. The laser head is approximately 100 kg with a dimension of $100 \times 40 \times 20$ cm^3.

The time interval of each part of the cylinder under the flashlamp pump must be less than the thermal time constant to keep uniform heating of the cylinder. When the laser operates at a 20 Hz repetition rate, i.e., the time interval for the same part of the glass cylinder to receive two adjacent pump pulses is 1 s, which is far less than the time constant for this cylinder. So the thermal effects of this rotating cylinder laser is well represented by the steady-state model. The system takes about 3 min to reach its stable performance.

Figure 5 shows the measured laser output energy versus pump input energy. When the two flashlamps are provided with 840 J electrical input energy per pulse, a maximum laser output energy of 21 J/pulse is obtained. Figure 6 shows the laser output power as a function of the average pump power when the pumping energy is kept at 620 J per pulse. The laser shows a linear relationship between output and input power, yielding a spatially multimode laser output of 305 W at a 19 Hz repetition rate, which is limited by the available power supply. The laser has an overall laser efficiency of 2.6%, and a slope efficiency of 3.8%. Higher efficiency can be expected from this system at higher pump energy density since the emission cross section of Nd:glass is small.

In the multimode operation, the maximum beam divergences at different pump powers are measured from the burn patterns on a piece of photographic paper. The laser beam is approximately rectangular in shape with a dimension of 8×28 mm^2 at highest power level. Cylinder motion has a negligible effect on beam pointing stability. In Figure 7 the product of the far-field half-angle θ (mrad) and the near-field beam half-width w (mm), which is defined as the beam parameter product, is plotted as a function of the average pump power when the pumping energy is kept at 620 J/pulse. Measurements show that the beam divergence along the radial direction ($//\theta$) correlates almost linearly with the average input power, but the divergence keeps almost the same value in the orthogonal plane ($\perp\theta$). When the laser provides 300 W average power output, the full-angle far-field beam divergence is measured to be 12.5×9 mrad. The difference in divergence in the two planes, as a result of non-zigzag beam propagation along z-axis through the cylinder, can be compensated

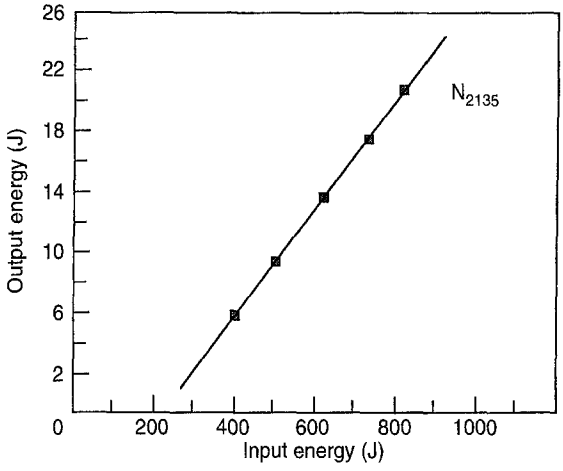

Fig. 5. Measured laser output energy versus flashlamp output energy. The overall efficiency is 2.6% and the slope efficiency is 3.8% for the 3.5% Nd doped glass laser

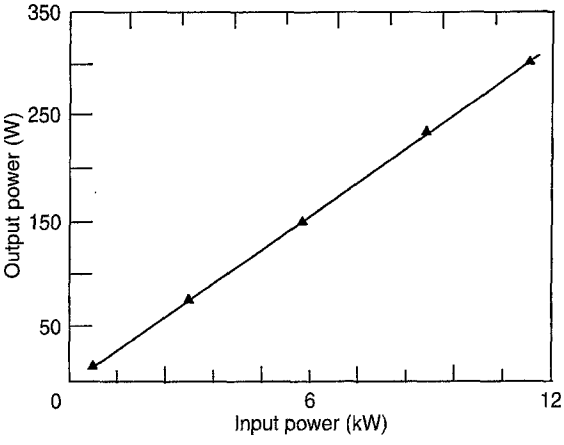

Fig. 6. Measured laser output power versus lamp input power for the 3.5% Nd doped glass laser. The laser is pumped by two flashlamps with a total energy of 620 J/pulse. The average power output is more than 300 W at a 19 Hz repetition rate

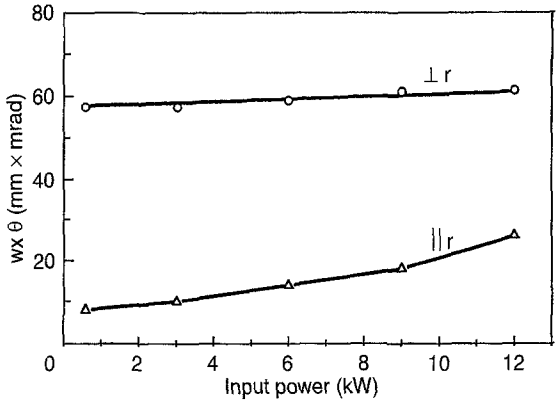

Fig. 7. The beam parameter product against the average pump power when the pumping energy is kept at 620 J per pulse

with the use of an intracavity optics [28]. This will lead to an improvement of output beam quality.

The maximum average output power per unit volume can be estimated according to (14),

$$\bar{P}_{\text{out}} = \eta \bar{P}_{\max}, \tag{17}$$

where $\eta = 2.6\%$, is the overall laser efficiency. Equation (17) gives $\bar{P}_{\text{out}} = 0.69\ \text{W/cm}^3$ for N_{2135} glass and $1.7\ \text{W/cm}^3$ for LHG-5 glass using the same design. The current laser has the capability of producing more than 0.5 kW laser output under the allowable thermal loading given by (14). On the basis of our investigations, a rotating laser scaling to kilowatt average power levels is possible. Using N_{335} glass, the same device could give a maximum output of 1 kW without stress fracture, compared with a value of R_S being two times bigger than N_{2135} glass.

3 Conclusions

The thermal model developed for a rotating hollow cylinder laser agrees well with measurements and provides useful information for the design of such a laser device. The results from a cylinder geometry laser can also apply to rod and slab geometry lasers, as two special cases. A rotating cylinder laser has been demonstrated to have a potential application for high average power operation of Nd:glass to kilowatt output power levels. Stable laser output energy of 300 W up to a 19 Hz repetition rate has been achieved at 2.6% overall efficiency and at 3.8% slope efficiency. The rotating cylinder laser without zigzag propagation of the beam reduces the cavity loss caused by multiple total internal reflection bounces and fabrication cost, but it is not so severely affected by the end effects and thermal deformations as the slab lasers without zigzag propagation of the beam [6].

References

1. J.T. Hunt and D.R. Speck: Opt. Eng. **28**, 461 (1989)
2. W.S. Martin and J.P. Chernoch: U.S. Patent 3 633 126, 1972
3. G.H. Hulme and W.B. Jones: Soc. Photo-Opt. Instr. Eng. **69**, 38 (1975)
4. J.M. Eggleston, T.J. Kane, K. Kuhn, J. Unternahrer and R.L. Byer: IEEE J. Quantum Electron. **QE-20**, 289 (1984)
5. T.J. Kane, J.M. Eggleston and R.L. Byer: IEEE J. Quantum Electron, **QE-21**, 1195 (1985)
6. Huang Guosong, Zhang Guoxuan, Zhou Feng, Gu Gencai and Gu Shaoting: Chinese J. Lasers, Special Issue on Laser Devices, 66 (1990)
7. T.J. Kane and R.L. Byer: J. Opt. Soc. Amer. **72**, 1755 (1982)
8. R.L. Byer: U.S. Patent 4 555 786, Nov 1985
9. S. Basu, T.J. Kane and R.L. Byer: IEEE J. Quantum Electron. **QE-22**, 2052 (1986)
10. S. Basu and R.L. Byer: Opt. Lett. **11**, 617 (1986)
11. D. Milam, and H. Schlossberg: J. Appl. Phys. **44**, 2297 (1973)
12. U. Wittrock, *High Power Rod, Slab and Tube Lasers*, Proc. NATO Advanced Study Institute on Solid State Lasers: New Developments and Applications, Eds. M. Inguscio and R. Wallenstein (Plenum Press, New York, 1993)
13. Y. Takada, H. Saito and T. Fukioka: Proc. Soc. Photo-Opt. Instrum. Eng. **801**, 62 (1987)
14. U. Wittrock, B. Eppich and H. Weber: Opt. Lett. **16**, 1092 (1991)
15. T. Korn, T.H. Jeys and T.Y. Fan: Opt. Lett. **16**, 1741 (1991)
16. H.S. Carslaw and J.C. Jarger: *Conduction of Heat in Solids* (Oxford Univ. Press, London 1959)
17. Zhou Feng, Zhang Guoxuan, Huang Guosong and Wang Zhijiang: Acta Physica Sinica **38**, 247 (1989)
18. W. Koechner: J. Appl. Phy. **44**, 3162 (1972)
19. S. Timoshenko and J.N. Goodier: *Theory of Elasticity* (McGram-Hill, New York, 1951)
20. W. Koechner: *Solid-State Laser Engineering* (Springer, New York, 1976)
21. Three types of 3.5% Nd doped glass N_{335}, N_{1035} and N_{2135} listed in Table 1 are manufactured by Shanghai Institute of Optics and Fine Mechanics, Chinese Academy of Sciences. As a comparison, material properties of LHG-5 (Hoya) are also listed.
22. Huang Guosong, Gu Shaoting and Gu Gencai: Chinese J. Lasers **18**, 885 (1991)
23. Zhu Congshan, Huang Guosong and Zhang Guoxuan: Chinese J. Lasers **18**, 507 (1991)
24. M. Born and E. Wolf: *Principles of Optics* (Pergamon, London 1965)
25. Huang Guosong, Zhou Feng, Gu Shaoting, Zhang Guoxuan and Chen Zexing: Acta Physica Sinica **39**, 367 (1990)
26. Zhou Feng, Zhang Guoxuan, Huang Guosong and Wang Zhijiang: Chinese J. Lasers. **17**, 65 (1990)
27. M. Reed, K. Kuhn, J. Unternahrer and R.L. Byer: IEEE J. Quantum Electron. **QE-21**, 412 (1985)
28. M. Reed and R.L. Byer: IEEE J. Quantum Electron. **QE-26**, 2138 (1990)